Backscatter model for the unusual radar properties of the Greenland Ice Sheet

Eric Rignot

Jet Propulsion Laboratory, Pasadena, CA

Abstract. A number of planetary objects exhibit unusual radar polarization properties and more recently a similar behavior has been observed over a vast portion of the Earth's surface: the percolation facies of the Greenland Ice Sheet. Surface-based ranging radar data and snow stratigraphy studies demonstrated that the unusual radar properties of that portion of Greenland are caused by enhanced scattering from massive, large, solid-ice bodies buried in the top few meters of the dry, cold, clean snowy surface of the ice sheet and created by seasonal melting and refreezing events. Here, we model the icy inclusions as randomly distributed, horizontal and nearly vertical, discrete, dielectric cylinders embedded in a transparent snow medium. An exact analytical solution is used to compute the scattered field from the cylinders. The model predictions are in good agreement with fully polarimetric radar observations gathered by an airborne imaging system simultaneously at three radar wavelengths (5.6, 24 and 68 cm) with an incidence angle of the radar illumination varying between 19 and 65 degrees. The diameter and number density of the cylinders that are inferred from the radar data using the backscatter model are consistent with in-situ observations of the icy inclusions. The large radar reflectivity and polarization ratios of the Greenland percolation facies are interpreted as arising from internal reflections of the radar signals in the icy inclusions that first-order scattering models fail to predict. The results compare favorably with predictions from the coherent backscatter or weak localization theory and may provide a complementary framework for interpreting exotic radar echoes from other planetary objects.

Submitted to *JGR Planets* on September 26, 1994.

1. INTRODUCTION

Since the early 1970's unusual radar properties have been detected from the icy Galilean satellites, Europa, Ganymede and Callisto (EGC) by Earth-based radar telescopes [*Ostro et al., 1992*]. Similar unusual radar characteristics have also been recorded from the Mars residual south polar cap [*Muhleman et al., 1991; Harmon et al., 1992*], portions of Titan [*Muhleman et al., 1990*], polar caps on Mercury [*Slade et al., 1992; Harmon and Slade, 1992*] and portions of Venus [*Tryka and Muhleman, 1992*]. First-order scattering models fail to explain the scattering behavior of these objects or are inconsistent with their history formation and geology [*Ostro and Shoemaker, 1990*]. Recently, the coherent backscatter effect [*e.g. van Albada et al., 1990; MacKintosh and John, 1988*], also known as weak localization theory, was suggested as a likely explanation for these radar echoes which was both consistent with their geology and capable of explaining their large polarization ratios and strong radar reflectivity [*Hapke, 1990*]. Detailed validation of the coherent backscatter theory, other than in laboratory-controlled experiment [*MacKintosh et al., 1989; Hapke and Blewett, 1991*], is however hampered by the absence of detailed, in-situ observations of the subsurface configurations responsible for the radar echoes from these planetary objects.

More recently, a similar behavior has been observed over a vast portion of the Earth's surface: the percolation facies of the Greenland Ice Sheet [*Rignot et al., 1993*]. The percolation facies represent a major fraction of the Greenland Ice Sheet which itself covers a 1,726,400 km^2 area [*Benson, 1962*]. It had been known for several years that the percolation facies exhibited an unusual strong type of radar backscattering [*Swift et al., 1985*], but it was not until 1991 that calibrated radar data could be gathered in that region, at three different wavelengths, multiple incidence angles and most importantly with the full polarimetry, using the NASA/Jet Propulsion Laboratory AIRSAR airborne synthetic-aperture radar imaging system [*van Zyl et al., 1992*].

The AIRSAR results showed that the circular and linear polarization ratios of the Green-

land percolation facies are extremely large and comparable in magnitude to the largest ratios recorded for EGC; and so is the magnitude of the radar echoes, making the Greenland percolation facies one of the brightest natural terrain of the Earth's surface at centimetric wavelengths. Analysis of signals recorded at 5.7 and 2.2 cm wavelength by a surface-based ranging radar deployed on the ice sheet at the time of the AIRSAR over flight demonstrated that the unusual radar echoes are caused by strong scattering from the first annual layer of ice bodies buried at depth (1-2 m) in the cold, dry, porous, snowy surface of the ice sheet [*Jezek and Gogineni, 1992; Jezek et al., 1994*]. Radar returns from the surface of the ice sheet as well as from deeper layers of ice bodies were estimated to be as much as 10 decibels weaker than that from the first layer of ice bodies.

These icy formations are well known to glaciologists [*Benson, 1962; Pfeffer et al, 1991; Jezek and Gogineni, 1992; Echelmeyer et al., 1992*]. They form in the top few meters of the snowy surface of the ice sheet as a result of seasonal melting and refreezing events. They differ from the glacial ice, 50 to 100 m underneath the surface, that results from diagenetic processes transforming snow into solid-ice. The physical processes yielding to the formation of the icy inclusions have been studied in great detail [*Benson, 1962; Pfeffer et al., 1990*]. At these high elevations ($\geq$ 2000 m a.m.s.l.) and high northern latitudes ($\geq 63^{o}$ N) snow remains at negative temperatures throughout the summer, except at point locations where melt-water can percolate downwards, along active channels, through much of the previous winter's accumulated snow. Melt-water refreezes at depth ($\leq$ 1 m) when it encounters a discontinuity in hydraulic conductivity associated to a fine-to-coarse grain size transition [*Pfeffer and Humphrey, 1992*]. When active, the percolation channels appear slushy. When refreezing, they form a network of ice pipes, lenses and layers that distribute laterally, sometimes over great distances. Ice lenses are lens-shaped layers which pinch out laterally, parallel to the firn strata; while ice pipes are pipe-like vertically extending masses reminiscent of the percolation channels which feed ice lenses and layers. Ice layers

are typically several millimeters to several centimeters thick and extend over several tens of meters. Ice pipes (Fig. 1) and ice lenses are 2-20 cm wide and 10-100 cm long [*Jezek et al., 1994*].

Ice layers also form at lower elevations, in the so-called soaked facies [*Benson, 1962*], but the snow there reaches 0°C in the summer, therefore is moist and not transparent to the radar signals which cannot interact with the buried solid-ice bodies. In winter, the melted snow refreezes to form a superimposed ice zone which forms a continuous, very thick, impermeable horizon of low radar reflectivity and small polarization ratios. Conversely, at higher elevations, in the deep interior of the ice sheet, in the so-called dry-snow facies [*Benson, 1962*], summer-melting rarely occurs and no icy formations are found in the top few meters of the snowy surface of the ice sheet. There, radar reflectivity and polarization ratios are as low as in the soaked-snow facies.

As for the icy Galilean satellites, the coherent backscatter effect was suggested as a possible explanation for the unusual radar properties of the Greenland percolation facies [*Rignot et al., 1993*]. The upper few meters of the ice sheet are sufficiently transparent to allow long photon path length and higher order scattering, contain an abundance of solid-ice scatterers at least as large as the radar wavelength, with a small relative refractive index, so coherent backscatter can dominate the radar echoes.

Here, we present a revision of our earlier hypothesis that the Greenland radar echoes are indeed explained by the coherent backscatter effect. We present a more detailed and quantitative investigation of the scattering mechanisms responsible for the Greenland radar echoes based on our knowledge of the subsurface configuration of the ice sheet and on the combined use of the calibrated, multi-parameter, AIRSAR radar data. In turn, we address the following three issues: Is there a backscatter model that can correctly and quantitatively mimic the radar properties of Greenland simultaneously at several radar frequencies, all polarizations and various incidence angles ? What kind of geophysical information can

orientation of the incident linear polarization (hence HV or VH = 0). In the case of volume scattering from randomly distributed dipoles, we have $\mu_C = 1$ and $\mu_L = 1/3$ [*Long, 1965*]. For pure double reflections off a perfectly smooth dielectric dihedral whose lower face is horizontal, $\mu_C = \infty$ (because RL = 0) and $\mu_L = 0$ (because HV = 0).

Also shown in Fig. 2 are the disk-integrated measures of the radar reflectivity and polarization ratios of EGC at 3.5- and 13-cm from Ostro et al. [*1980, 1992*]. Both EGC and the Greenland percolation facies exhibit strong radar reflectivity, $\mu_C > 1$ and $\mu_L > 1/3$. Most natural terrestrial surfaces and Inner Solar System planetary bodies exhibit lower radar reflectivities, $\mu_C << 1$ and $\mu_L << 1/3$.

To illustrate the discussion with real examples, several AIRSAR measurements of heavily vegetated areas (forests) and very rough surfaces (lava flows) are included in Fig. 2. In broadleaf-upland tropical rain forest in Belize (-17.58 deg. North, 89.0 deg. West) [*Freeman et al., 1992*], the AIRSAR results show $\mu_C \approx 1$ and $\mu_L \approx 1/3$ at 24- and 68-cm and σ°_{OC} is several orders of magnitude lower than that recorded for Greenland at the same incidence. The values of the polarization ratios are consistent with scattering dominance by the tree branches of the forest canopy which act as randomly distributed thin cylinders or dipoles. At 5.6-cm, $\mu_C < 1$ and $\mu_L < 1/3$ because the branches are no longer thin compared with the observing wavelength. There are however numerous cases of forested areas where $\mu_C > 1$ at the longer wavelengths. For instance, in palm-tree communities of the Manu National Park tropical rain forest, in Peru (-11.98 deg. North, 70.8 deg. West) AIRSAR measured $\mu_C > 1.5$ and $\mu_L < 0.1$ at 68-cm, yet σ°_{OC} is much lower than that for Greenland. We interpret this behavior as caused by double-bounce reflections of the radar signals from the tree-trunks to the flooded ground back to the radar direction. Double-bounce scattering increases with increasing tree height [*van Zyl, 1993*] (hence is largest for tall forest), increasing wetness of the ground layers and/or of the tree-trunks (hence largest for flooded forest) and increasing radar penetration (hence largest at the longer wavelengths

and/or for sparser forests). Double-bounce reflections preserve the handedness of the helicity of the incident circular polarization, so μ_C may become greater than unity, and preserve the orientation of the incident linear polarization - unless the tree-trunks are no-longer vertical and significantly slanted or damaged [*van Zyl, 1993*] - so $\mu_L < 1/3$. This example illustrates the importance of measuring the complete scattering matrix to characterize the nature of scattering. With only μ_C and σ^o_{OC}, the radar signature of flooded forests, but also of very tall forests or sparse forests, could be misinterpreted as resulting from the coherent backscatter effect simply because $\mu_C > 1$.

Enhanced radar backscatter and strong depolarization of the radar signals may also occur on surfaces that are very rough at the scale of the radar wavelength for instance through multiple reflections of the radar signals on the large facets of blocky structure of the surface. Several authors [*Fahnenstock et al. 1993; Jezek et al., 1994*] in fact argued that the unusual radar properties of the Greenland percolation facies are caused by surface scattering from the rough ice layers. To determine whether this is a valid explanation we examined the radar response of several types of very rough surfaces and experimented with theoretical backscatter models.

Lava flows are good examples of very rough surfaces. Fig. 2 shows samples of radar echoes from Qb3 lava flow (quaternary volcanic basalt flow - younger type) of the Lunar Crater Volcanic Field (38.47 deg. North, 116.07 deg. West), in the Mojave Desert, Nevada [*Evans et al., 1992; Scott and Trask, 1971*]. The rms height of the surface was estimated from stereo imagery to be about 24 cm. At 30 degrees incidence, σ^o_{OC} is several orders of magnitude lower than that recorded in Greenland, $\mu_C < 1$ and $\mu_L < 1/3$. This example suggest that rough surfaces are unlikely to exhibit exotic radar characteristics. Circular polarization ratios greater than unity have however been reported in SP flow of northern Arizona (35.8 deg. North, 117.42 deg. West) [*Campbell et al., 1993*], also shown in Fig. 2. SP flow is a blocky basaltic andesite lava deposit whose surface is characterized by roughly cubical

blocks 10-100 cm in size and whose sides are smooth on the scale of a few centimeters. Their radar scattering behavior is likely attributed to the dihedral double-bounce phenomenon discussed above and not to coherent backscatter because the refractive index of rock in air is too large to yield coherent backscattering [*Peters, 1992; Mishchenko, 1992*]. Interestingly, $\mu_L > 1/3$ in SP flow at 24-cm, which suggests that the dihedrals formed by the large facets of the blocky structure of the surface are randomly oriented. At 68-cm the polarization ratios are lower, which suggests that most basaltic andesite blocks that form the surface are less than 0.7 m in size. Recent AIRSAR observations of the Inyo-Mono lava domes, in California (37.7 deg. North, 119.1 deg. West) [*Plaut et al., 1993*], where surface rms heights reach 83 cm, confirm that in the presence of extremely rough surfaces multiple-bounce scattering from the large facets of blocky structure eventually dominates scattering from small-scale roughness at the longer wavelengths (24- and 68-cm), but the corresponding radar signatures are not exotic ($\sigma^o_{OC} << 1$, $\mu_C < 1$ and $\mu_L < 1/3$ in Fig. 2).

Radar scattering models for randomly rough dielectric surfaces are usually not valid over the complete range of surface roughness values encountered in natural terrain settings. One of the most comprehensive model todate is the Integral Equation Method, IEM [*Fung et al., 1992*]. The IEM model unites the small perturbation model [*Rice, 1951*] for slightly rough surfaces and the Kirchhoff theory for very rough surfaces. We tested the IEM model using the roughness values measured with a mechanical comb gauge at the surface of an ice layer (3-cm rms height and 3-cm correlation length [*Jezek et al., 1994*]). The results, shown in Fig. 3, illustrate the incompatibility of the model predictions with the AIRSAR observations. The contrast between 5.6- and 24-cm echoes is over predicted and the modeled radar reflectivity at small incidence is several decibels below that recorded for Greenland. Hence, the IEM model predictions, together with numerous radar observations of rough terrestrial surfaces (Fig. 2), demonstrate that surface scattering from the ice layers is not capable of explaining the radar characteristics of Greenland.

3. A BACKSCATTER MODEL FOR THE PERCOLATION FACIES

One common deficiency of many backscatter models is that they are only approximations to the exact solution of the scattered field from the scattering objects. Higher-order modes of interactions of the radar signals with the objects are simply ignored. Although this simplification is justified for most natural targets, it is not the case for Greenland where higher-order scattering terms are predominant.

The exact solution of the scattered field from dielectric objects exist for a few simple objects such as spheres and cylinders. Here, we use discrete, dielectric cylinders to model the icy inclusions of the percolation facies. The ice layers are not represented as we assume that they are too thin compared with the observing wavelength to scatter the incoming radar signals efficiently. Although the ice pipes and lenses are not pure cylinders of solid-ice (Fig. 1 shows their diameter is not constant), modeling them as, respectively, vertical and horizontal cylinders at the level of spatial details of one wavelength is reasonable. In this manner we account for the anisotropy of these objects, their geometrical shape, their spatial distribution and orientation and their electrical properties. Because ice pipes and lenses are often separated by more than one wavelength, we will also assume that the scattered field from these objects is uncorrelated so that the total radar backscatter from a distribution of discrete, dielectric cylinders can be computed as the incoherent sum of the scattered field from the individual cylinders. Also, because ice pipes and ice lenses are neither purely vertical nor purely horizontal, we assume that the nearly-vertical cylinders are randomly oriented within $\pm\delta\theta = 5$ degrees in the plane of incidence and within $\pm\alpha_o$ in the vertical plane (plane containing the velocity vector of the aircraft and the normal to the surface). For the horizontal cylinders, we use $\delta\theta = 5$ degrees in the plane of incidence and $\alpha_o = \pi/2$ in the horizontal plane, i.e. randomly oriented cylinders in the horizontal plane. The random orientation in the plane of incidence merely results in a smoothing of the

radar characteristics versus the incidence angle of the radar illumination. Using 5 degrees provided a reasonable degree of smoothing while being consistent with field observations; but this value should by no means be considered as a critical value. In contrast, the random orientation of the cylinders in the vertical or horizontal plane, characterized by α_o, has a more fundamental importance that is discussed in the next few paragraphs.

The absorption properties of dry, cold snow are assumed to be negligible. Snow is nearly transparent to radar signals at those wavelengths. The radar backscatter of the top of the snowy surface of the ice sheet was estimated to be more than 10 decibels below that recorded for the icy bodies, even at 2.2-cm wavelength [*Jezek et al., 1994*]. Snow however steepens the incidence angle of the radar illumination through refraction of the radar signals at the air-snow interface, reduces the dielectric constant of water-ice in dry air ($\epsilon = 3.2$) to a lower value corresponding to water-ice in dry snow ($\epsilon = 1.78$ for a snow density of 0.4 kg/m^3 [*Tiuri et al., 1984*]) and reduces the effective wavelength of the radar signals by about 25% (or $\sqrt{(\epsilon)}$).

The exact scattering matrix for a dielectric cylinder of infinite length is given in Bohren and Huffman [*1983*]. The analytical solution for a finite cylinder is computed by scaling the solution for the infinite cylinder by a shape factor

$$f = \frac{kh}{\pi} sin_c(k\ h\ cos\ \theta) \tag{2}$$

where k is the wavenumber, h is the cylinder length, θ the incidence angle of the radar illumination and $sin_c(x) = sin(x)/x$. If the cylinder length varies randomly by a quantity $\pm\epsilon_h$, the average solution for the scattered field intensity is obtained by integrating f^2 between $h - \epsilon_h$ and $h + \epsilon_h$. When ϵ_h is larger than one wavelength the result is

$$< f^2 >= \frac{1}{2\pi^2 cos^2\theta}, \tag{3}$$

which is independent of both h and ϵ_h. Hence, when the cylinder length fluctuates by $\sim \lambda$, the mean value of the cylinder length has no influence on the radar characteristics of the

cylinder. Given the typical sizes of ice pipes and lenses, this condition is easily satisfied at 5.6- and 24-cm and we assume it also applies at 68-cm. Hence the shape factor f only intervenes in the model as a $cos^{-2}\theta$ multiplicative term of the signal intensity.

We now examine how to compute the scattered field from randomly distributed discrete, dielectric cylinders, given the solution for one cylinder. The scattering matrix $[S] = [S_{HH}, S_{HV}, S_{VH}, S_{VV}]$ of a single dielectric cylinder oriented horizontally can be written as

$$[S] = [a, 0, 0, b] \tag{4}$$

where a and b are complex numbers whose magnitude and phases are functions of the cylinder dielectric constant and diameter [*Bohren and Huffman, 1983*]. To calculate the average covariance matrix for nearly-vertical (horizontal) cylinders randomly oriented at about an angle $\pm\alpha_o$ in the vertical (horizontal) plane, we apply a rotation operator to $[S]$ and average the results over all angles between $-\alpha_o$ and $+\alpha_o$. The resulting average cross-products of the scattering matrix are

$$< S_{HV}S_{HV}* >=\mid a-b \mid^2 I_{22} \tag{5}$$

$$< S_{HH}S_{HH}* >= (\mid a \mid^2 + \mid b \mid^2)I_4 + 2Re(a^*b)I_{22} \tag{6}$$

$$< S_{VV}S_{VV}* >=< S_{HH}S_{HH}* > \tag{7}$$

$$< S_{HH}S_{VV}* >= (\mid a \mid^2 + \mid b \mid^2)I_{22} + 2Re(a^*b)I_4 \tag{8}$$

$$\text{where} \quad I_4 = \int_{-\alpha_o}^{\alpha_o} cos^4(\alpha)d\alpha \quad \text{and} \quad I_{22} = \int_{-\alpha_o}^{\alpha_o} cos^2(\alpha)sin^2(\alpha)d\alpha \tag{9}$$

At circular polarization, the cross-products are

$$< S_{RR}S_{RR}* >= \frac{1}{2}(I_4 + I_{22}) \mid a-b \mid^2 \tag{10}$$

$$< S_{LL}S_{LL}* >=< S_{RR}S_{RR}* > \tag{11}$$

$$< S_{RL}S_{RL}* >= \frac{1}{2}(I_4 - I_{22}) \mid a+b \mid^2 + I_{22} \mid a-b \mid^2 \tag{12}$$

from which we compute the polarization ratios, $\mu_C =< S_{RR}S_{RR}* > / < S_{RL}S_{RL}* >$ and $\mu_L =< S_{HV}S_{HV}* > / < S_{HH}S_{HH}* >$.

When $\alpha_o = \pi/2$ and b approaches zero (thin cylinder limit), we find $\mu_C = 1$ and $\mu_L = 1/3$ as for the case of scattering from a forest canopy where branches are thin compared to the wavelength. When $\mid b \mid$ approaches $\mid a \mid$ (thick cylinder limit), we find $\mu_C = 0$ and $\mu_L = 0$, as expected since $[S]$ becomes the identify matrix. When $a = -1$ and $b = 1$ (case of a dihedral reflector), we find $\mu_C = (I_4 + I_{22})/(2\, I_{22})$ and $\mu_L = I_{22}/(I_4 - I_{22})$. Hence large polarization ratios may be obtained from a distribution of randomly oriented dihedrals ($\mu_C = 2$ and $\mu_L = 0.5$ when $\alpha_0 = \pi/2$), which could be a reasonable explanation for the large polarization ratios recorded in SP flow [*Campbell et al., 1993*].

When $\alpha_o = 0$ (purely vertical cylinders), we find $\mu_L = 0$ and $\mu_C = \mid \frac{a-b}{a+b} \mid^2$. Hence, dielectric cylinders do not generate any cross-polarized intensity unless they are randomly oriented. For the ice lenses, the random orientation of the cylinders is obvious since the ice lenses have no preferred orientation in the horizontal plane. For the ice pipes, we assume that the randomness in orientation reflects spatial irregularities in shape and orientation of the ice pipes along their longest dimension at a scale comparable to or larger than the wavelength (Fig. 1).

Using this backscatter model we are able to predict large polarization ratios for the icy inclusions. To get some insight into the nature of this scattering behavior we plotted the radar reflectivity and polarization ratios of various sized-cylinders in Fig. 4a-d. Narrow peaks in μ_C and μ_L are observed for particular values of the cylinder radius, which coincide with HH-VV phase differences of about 180 degrees. These peaks are caused by internal reflections of the radar signals in the cylinders, which includes the glory ray effect discussed in [*Bohren and Huffman, 1983*] as well as other types of internal reflection processes that are included in the exact analytical solution to the scattered field. Internal reflections are the only type of returns that would cause a large phase difference between HH-polarized and VV-polarized radar signals. As the refractive index of the cylinder increases, it is expected that these internal reflections are less likely to occur. An example is shown in Fig. 4e-h,

When $\alpha_o = \pi/2$ and b approaches zero (thin cylinder limit), we find $\mu_C = 1$ and $\mu_L = 1/3$ as for the case of scattering from a forest canopy where branches are thin compared to the wavelength. When $\mid b \mid$ approaches $\mid a \mid$ (thick cylinder limit), we find $\mu_C = 0$ and $\mu_L = 0$, as expected since $[S]$ becomes the identify matrix. When $a = -1$ and $b = 1$ (case of a dihedral reflector), we find $\mu_C = (I_4 + I_{22})/(2\, I_{22})$ and $\mu_L = I_{22}/(I_4 - I_{22})$. Hence large polarization ratios may be obtained from a distribution of randomly oriented dihedrals ($\mu_C = 2$ and $\mu_L = 0.5$ when $\alpha_0 = \pi/2$), which could be a reasonable explanation for the large polarization ratios recorded in SP flow [*Campbell et al., 1993*].

When $\alpha_o = 0$ (purely vertical cylinders), we find $\mu_L = 0$ and $\mu_C = \mid \frac{a-b}{a+b} \mid^2$. Hence, dielectric cylinders do not generate any cross-polarized intensity unless they are randomly oriented. For the ice lenses, the random orientation of the cylinders is obvious since the ice lenses have no preferred orientation in the horizontal plane. For the ice pipes, we assume that the randomness in orientation reflects spatial irregularities in shape and orientation of the ice pipes along their longest dimension at a scale comparable to or larger than the wavelength (Fig. 1).

Using this backscatter model we are able to predict large polarization ratios for the icy inclusions. To get some insight into the nature of this scattering behavior we plotted the radar reflectivity and polarization ratios of various sized-cylinders in Fig. 4a-d. Narrow peaks in μ_C and μ_L are observed for particular values of the cylinder radius, which coincide with HH-VV phase differences of about 180 degrees. These peaks are caused by internal reflections of the radar signals in the cylinders, which includes the glory ray effect discussed in [*Bohren and Huffman, 1983*] as well as other types of internal reflection processes that are included in the exact analytical solution to the scattered field. Internal reflections are the only type of returns that would cause a large phase difference between HH-polarized and VV-polarized radar signals. As the refractive index of the cylinder increases, it is expected that these internal reflections are less likely to occur. An example is shown in Fig. 4e-h,

for water-ice cylinders in vacuum (refractive index $\sim$ 1.8), where the peaks are strongly attenuated. Hence the refractive index of the cylinders needs to be small enough (typically less than 1.6) to yield large polarization ratios.

Model predictions for an ensemble of horizontal and vertical cylinders are shown in Fig. 5 along with the AIRSAR data. Several model parameters were adjusted to best fit the model predictions with the AIRSAR data. These parameters are: the radius and number density of vertical and horizontal cylinders and the angle distribution α_o of the vertical cylinders. The number densities were adjusted based on the values of σ^o_{OC} as σ^o_{OC} was found to be proportional to the density of horizontal cylinders at small incidence and proportional to the density of vertical cylinders at high incidence. We note here that with vertical cylinders only or horizontal cylinders only, the model would not be able to predict the correct trend of the polarization ratios versus the incidence angle. The vertical cylinder radius was determined from the values of the polarization ratios at high incidence. The horizontal cylinder radius was assumed to be equal to that of the vertical cylinders. The angle α_o was adjusted to properly balance μ_L and μ_C since these ratios vary in opposite directions when α_o is change. Because of the relative large number of constraints provided by the multi-parameter radar data, we typically only found one nearly optimal configuration at each radar wavelength to best match the AIRSAR observations.

At 5.6 cm wavelength, the model predictions are most accurate with cylinders about 6.2 cm in diameter, 5 vertical cyl/m^2 (cylinder per square meter) with α_o =70 degrees, and 1.5 horizontal cyl/m^2. Snow stratigraphy studies reveal that ice pipes are several tens of centimeters long and of diameter varying anywhere between 2-4 cm to 10-20 cm. The number density of icy inclusions was not measured per se - such measurement would require the digging of a large number of snow pits - but the results of snow stratigraphy studies suggest that a few pipes and lenses per square meter is a reasonable number. Hence the model results are consistent with in-situ observations.

At 24-cm, cylinders have to be 17.8 cm in diameter (1 vertical cyl/m^2 with α_o =50 degrees and 3 horizontal cyl/m^2) to yield a good agreement between radar observations and model predictions. Field observations suggest this value may be at the limit of being too large to represent an ice pipe. Perhaps the result should be interpreted as the diameter of the icy inclusions at the point of connection of an ice pipe with an ice lens, which is usually wider than the ice pipe itself.

At 68-cm, the polarization ratios and radar reflectivity are always low for cylinder diameters between 6.2 and 17.8 cm and would be large only if the icy inclusions could reach 30-40 cm in diameter. Indeed icy inclusions are never this large and both the model and the radar observations at 68-cm are consistent with the typical size of the inclusions.

4. DISCUSSION

The modeling results demonstrate that internal reflection processes of the radar signals in horizontal and vertical, discrete, solid-ice inclusions buried in the snowy, radar-transparent, surface of the ice sheet can explain the extraordinary radar properties of the Greenland percolation facies. The model predictions from a rather simple backscatter model that includes all scattering terms from a cylinder are in good agreement with radar observations gathered at various incidence angles, three different wavelengths and all polarizations by an airborne imaging radar system. The model also provide a description of the size and number density of these objects that is consistent with in-situ measurements. Further studies of the radius and number density of these objects are needed to establish more completely the accuracy of the inversion results. On the other hand, the model provides no information on the length of the cylinders. Additional constraints on the aspect ratio of these objects are needed before glaciologists can estimate the (unknown) volume of ice retained in the ice sheet by seasonal melting from the radar data and revise current estimates of the mass balance of the ice sheet [*Pfeffer et al., 1990*].

Several backscatter models have been proposed in the past to explain unusual radar echoes from planetary surfaces. The mode-decoupled refraction scattering [*Hagfors et al., 1985; Eshelman, 1986*] would not apply for Greenland because it requires exotic subsurface structures that do not exist. But the total-internal reflection model [*Goldstein and Green, 1980*] is similar to our model. The major difference is that here we use a complete solution of the scattered field, and henceforth are able to determine under which circumstances all internal reflection processes may dominate other forms of scattering and by what amount. For instance, the present model predicts that internal reflections in pure water-ice cylinders in vacuum would not likely yield $\mu_C > 1$ (Fig. 4).

In the coherent backscatter theory, enhanced radar backscatter and large polarization ratios result from constructive interactions between radar signals traveling in time-reversed paths through a weakly absorbing medium which contains closely-spaced ($\sim \lambda$) forward scatterers [*e.g. van Albada et al., 1990*]. The scatterers need to be large in size compared with the observing wavelength and of small refractive index for the coherent backscatter effect to take place [*Peters, 1992; Mishchenko, 1992*]. There is no requirement on the geometrical shape of the scatterers so most numerical computer models and laboratory experiments have used spherical scatterers. The present model also requires scatterers embedded in a weakly absorbing medium, large in size compared with the observing wavelength and of small refractive index. In addition, we require discrete discontinuities in dielectric constant resembling cylinders, randomly oriented and, in the case of Greenland, both nearly-vertical and horizontal. The scatterers do not need to be closely-spaced however and in-situ observations of the subsurface configuration of the ice sheet show that icy inclusions are often separated by many wavelengths, in which case the coherent backscatter effect may not take place. In addition, model predictions from the coherent backscatter theory suggest that μ_C and μ_L should decrease with an increasing incidence angle (Fig. 6,15 and 9,18, [*Mishchenko, 1992*]) whereas the AIRSAR measurements show an opposite trend. Hence, we conclude

that in the case of the Greenland percolation facies, internal reflection processes from the discrete icy inclusions is a more likely explanation for the unusual radar echoes than coherent backscattering from a random distribution of icy inclusions.

In the case of other planetary objects the conclusions may be different. The possibility of having planetary objects with regolith structures containing large, discrete, cylinder-like, inclusions has been deemed unfavorable by Ostro and Shoemaker [*1980*]. The coherent backscatter effect may then be the only plausible explanation for the radar echoes. In effect, in Peters' [*1992*] formulation of the coherent backscatter effect, the fluctuations in dielectric constant responsible for scattering are random in nature, which means that they could correspond to discrete discontinuities as well as random modulations in dielectric constant in a smoothly heterogeneous icy regolith. Otherwise, the present study illustrates that the coherent backscatter effect is not the only possible explanation for exotic radar echoes. In the case of the Greenland percolation facies, but also for very rough volcanic structures and flooded, tall or sparse forests that exhibit unusually large polarization ratios, the coherent backscatter effect is in fact not the explanation for the radar echoes. For extra-terrestrial objects, resolving the issue of whether coherent backscattering or internal reflection processes dominate scattering would be extremely difficult to settle without in-situ subsurface observations of the planetary surfaces. The most important problem remains to determine what geophysical information can be extracted from the radar data using these models and eventually confront the results from different theories. In that regard, the results of this study are very encouraging but multi-parameter radar data are essential.

Acknowledgements. I thank Jakob van Zyl for stimulating discussions during the course of this study and for providing a computer code calculating the scattering matrix of a finite cylinder; Kenneth Jezek and Carl Benson for valuable discussions on snow stratigraphy studies in Greenland; Jian Cheng Shi for providing his implementation of the IEM model; and Jeffrey Plaut for sharing his AIRSAR observations of the Inyo-Mono domes. This work was carried out at the Jet Propulsion Laboratory, California Institute of Technology, under contract with the Polar Research Branch of the National Aeronautics and Space Administration.

References

Benson, C., Stratigraphic studies of the snow and firn of the Greenland ice sheet, US Army Snow Ice and Permafrost Res. Estab., Research Report 70, 1962.

Bohren, C. F., and D. R., Huffman, *Absorption and Scattering of Light by Small Particles*, Wiley, NY, 1983.

Campbell, B.A., R. E. Arvidson, and M. K. Shepard, Radar polarization properties of volcanic and playa surfaces: Applications to terrestrial remote sensing and Venus data interpretation, *J. Geophys. Res., 98*, 17,099-17,113, 1993.

Echelmeyer, K., W. D. Harrison, T. S. Clarke, and C. Benson, Surficial glaciology of Jakobshavns Isbrae, West Greenland: Part II. Ablation, accumulation and temperature, *J. of Glaciology, 38*, 169, 1992.

Eshelman, V.R. , Mode decoupling during retrorefraction as an explanation for bizarre radar echoes from icy moons, *Nature, 319*, 755-757, 1986.

Evans, D.L., Farr, T.G., and J.J. van Zyl, Estimates of surface roughness derived from synthetic-aperture radar (SAR) data, *IEEE Trans. on Geosc. and Rem. Sens., 30*, 382-389, 1992.

Fahnenstock, M. , R. Bindschadler, R. Kwok and K. Jezek, Greenland Ice Sheet surface properties and ice dynamics from ERS-1 SAR imagery, *Science, 262*, 1530-1534, 1993.

Freeman, A., S. Durden, and R. Zimmermann, Mapping of sub-tropical vegetation using multi-frequency, multi-polarization SAR data, *Proc. of the Int. Geosc. and Rem. Sens. Symp., Houston, Texas, May 26-29, 1992, IEEE New York Pub.*, 1686, 1992.

Fung, A.K., L. Zongqian, and K.S. Chen, Backscattering from a randomly rough dielectric surface, *IEEE Trans. on Geosc. and Rem. Sens., 30*, 356-369, 1992.

Goldstein, R.M. and R.R. Green, Ganymede: radar surface characteristics, *Science, 207*, 179, 1980.

Hagfors, T. , T. Gold and M. Ierkic, Refraction scattering as origin of the anomalous radar returns of Jupiter's satellites, *Nature, 315*, 637-640, 1985.

Harmon, J.K., M.A. Slade, and R.S. Hudson, Mars radar scattering: Arecibo/Goldstone results at 12.6-cm and 3.5-cm wavelengths, *Icarus, 98*, 240, 1992.

Harmon, J.K. and M.A. Slade, Radar mapping of Mercury: full-disk images and polar anomalies, *Science, 258*, 640, 1992.

Hapke, B., Coherent backscatter and the radar characteristics of outer planet satellites, *Icarus, 88*, 407-417, 1990.

Hapke, B. and D. Blewett, Coherent backscattering model for the unusual radar reflectivity of icy satellites, *Nature, 352*, 46, 1991.

Jezek, K.C., S.P. Gogineni, and M. Shanbleh, Radar Measurements of melt zones on the Greenland Ice Sheet, *Geophys. Res. Letters* **21**, 33-36, 1994.

Long, M.W., On the polarization and the wavelength dependence of sea echo, *Trans. IEEE AP-14*, 749, 1965.

MacKintosh, F.C. and S. John, Coherent backscattering of light in the presence of time-reversal-noninvariant and parity-nonconserving media, *Phys. Rev. B, 37*, 1884, 1988.

MacKintosh, F.C., J.X. Zhu, D.J. Pine and D.A. Weitz, Polarization memory of multiply scattered light, *Phys. Rev. B, 40*, 2383, 1989.

Mishchenko, M.I., Enhanced backscattering of polarized light from discrete random media: calculations in exactly the backscattering direction, *J. Opt. Soc. Am., 9*, 978, 1992.

Muhleman, D.O., B.J. Butler, A.W. Grossman, and M.A. Slade, Radar images of Mars, *Science, 253*, 1508, 1991.

Muhleman, D.O., A.W. Grossman, B.J. Butler, and M.A. Slade, Radar reflectivity of Titan, *Science, 248*, 975, 1990.

Ostro, S.J., *et al.*, Europa, Ganymede, and Callisto: New radar results from Arecibo and Goldstone, *J. Geophys. Res., 97*, 18,227-18,244, 1992.

Ostro, S.J. and E.M. Shoemaker, The extraordinary radar echoes from Europa, Ganymede, and Callisto: a geological perspective, *Icarus, 85*, 335, 1990.

Ostro, S.J. , D. B. Campbell, G. H. Pettengill and I. I. Shapiro, Radar observations of the icy Galilean satellites, *Icarus, 44*, 431-440, 1980.

Peters, K.J., The coherent backscatter effect: a vector formulation accounting for polarization and absorption effects of small and large scatterers, *Phys. Rev. B, 46*, 801, 1992.

Pfeffer, W. T., T. H. Illangasekare, and M. F. Meier, Analysis and modeling of melt-water refreezing in dry snow, *J. of Glaciology, 36*, 238-246, 1990.

Pfeffer, W. T., M. F. Meier, and T. H. Illangasekare, Retention of Greenland runoff by refreezing: Implications for projected future sea level change, *J. Geophys. Res., 96*, C12, 22,117-22,124, 1991.

Pfeffer, W.T. and N.F. Humphrey, Initiation of ice piping and ice layering in subfreezing snow, in *Proc. AGU 1992 Fall Meeting*, H31D-4, 194, 1992.

Plaut, J.J., E. R. Stofan, D.A. Crown, S.W. Anderson, Steep-sided volcanic domes on Venus and Earth: Macro-scale geometry from remote sensing and field measurements, *EOS Trans., Am. Geo. Un., 74* 43, 1993.

Rice, S. O. 1951. Reflection of electromagnetic waves from slightly rough surfaces, *Commun. Pure Appl. Math., 4*, 351-378.

Rignot, E., S.J. Ostro, J.J. van Zyl, and K.C. Jezek, Unusual radar echoes from the Greenland Ice Sheet, *Science, 261*, 1710-1713, 1993.

Scott, D.H., and Trask N.J., Geology of the Lunar Crater Volcanic field, Nye County, NV, U.S. Geological Survey Professional Paper 599-I, 1971.

Slade, M.A., B.J. Butler and D.O. Muhleman, Mercury radar imaging: evidence for polar ice, *Science, 252*, 252, 1992.

Swift, C. T., P. S. Hayes, and J. S. Herd, Airborne microwave measurements of the southern Greenland ice sheet, *J. Geophys. Res., 90* B2, 1983-1994, 1985.

Tiuri, M., A.H. Sihvola, E.G. Nyfors and M.T. Hallikainen, The complex dielectric constant of snow at microwave frequencies, *IEEE J. Oceanic Engin., OE-9*, 377-382, 1984.

Tryka, K.A., and D.O. Muhleman, Reflection and emission properties on Venus: Alpha Regio, *J. Geophys. Res., 97*, 13,379, 1992.

van Albada, M.P., M.B. van der Mark, and A. Lagendijk, Experiments on weak localization of light and their interpretation, in *Scattering and Localization of Classifical Waves in Random Media*, Ed. by P. Sheng (World Scientific, Singapore), p. 97, 1990.

van Zyl, J. J., R. Carande, Y. Lou, T. Miller and K. Wheeler, The NASA/JPL three-frequency polarimetric AIRSAR system, *Proc. Int. Geosc. and Rem. Sens. Symp.*, Houston, Texas, May 26-29, 1992, IEEE New York Pub., 649-651, 1992.

van Zyl, J. J., The effect of topography on radar scattering from vegetated areas, *IEEE Trans. on Geosc. and Rem. Sens., 31*, 153-160, 1993.

E. Rignot, Jet Propulsion Laboratory, MS 300-243, 4800 Oak Grove Drive, Pasadena, CA 91109-8099. (e-mail: eric@adelie.jpl.nasa.gov)

List of Figures

Figure 1. Photograph of an ice pipe found at 1.80 m depth in the firn at Crawford Point on June 11, 1991. The ice pipe is 70 cm long and between 3 and 10 cm in diameter. (Courtesy of K. Jezek)

Figure 2. OC radar reflectivity σ^0_{RL}, circular polarization ratio μ_C and linear polarization ratio μ_L recorded at Crawford Point at 5.6-(red curve), 24-(blue curve), and 68-cm (green curve) as a function of the incidence angle of the radar illumination onto the reflecting surface. The plot also includes disk-integrated values of σ^0_{OC} and μ_C recorded at 3.5- (red squares) and 13-cm (blue squares) for EGC [*Ostro et al., 1992*]; μ_L for EGC at 3.5-cm only (red squares) [*Ostro et al., 1980*]; as well as σ^0_{RL}, μ_C and μ_L for broadleaf-upland tropical rain forest, in Belize (open circles) [*Freeman et al., 1992*]; for palm-tree stands from the tropical rain forest of the Manu National Park, in Peru (triangles); for Qb3 rough lava flows of the Lunar Crater Volcanic Fields, Nevada [*Evans et al., 1992*] (cross marks); and for the Inyo-Mono volcanic domes, California [*Plaut et al., 1993*] (plus signs). For the SL lava flows of northern Arizona only μ_C and μ_L are shown at 24- (blue filled circles) and 68-cm (green filled circles) because the radar data were not absolutely calibrated. 5.6-cm radar echoes are not used because of an erroneous antenna pattern correction. The data points for EGC are arbitrarily placed outside the plot along the horizontal axis (at a 69 degrees incidence) as they correspond to disk-integrated values.

Figure 3. Backscatter model predictions of the radar reflectivity at HH-polarization from the IEM theory (continuous lines) compared to the AIRSAR measurements (dotted lines) at 5.6-(red), 24-(blue), and 68-cm (green) versus the incidence angle of the radar illumination. The surface rms height is 3-cm with a 3-cm correlation length.

Figure 4. Polarization ratios, OC radar reflectivity and HH-VV phase difference for dielectric finite cylinders with (a) $\epsilon_r = 1.78$ (solid-ice in dry snow); (b) $\epsilon_r = 3.2$ (solid-ice in vacuum) as a function of $(k\ a)$ where k is the wavenumber and a is the cylinder radius. The letters P- (68-cm), L- (24-cm), and C- (5.6-cm) indicate the values of $(k\ a)$ for $a = 3.1$ cm which is the optimal cylinder radius to interpret the AIRSAR measurements at 5.6-cm.

Figure 5. Model predictions for discrete, nearly-vertical and horizontal, dielectric cylinders (continuous lines) compared to the AIRSAR measurements (dotted lines) at 5.6- (red), 24-(blue), and 68-cm (green). At 5.6-cm, we use $a = 3.1 \pm 0.05$ cm; $\alpha_o = 70$ degrees; $\delta\theta = 5$ degrees; 5 vertical cyl/m^2; 1.5 horizontal cyl/m^2. At 24- and 68-cm we used $a = 8.9 \pm 0.05$ cm; $\alpha_o = 50$ degrees; $\delta\theta = 5$ degrees; 1 vertical cyl/m^2; 3 horizontal cyl/m^2.

RIGNOT FIGURE 1

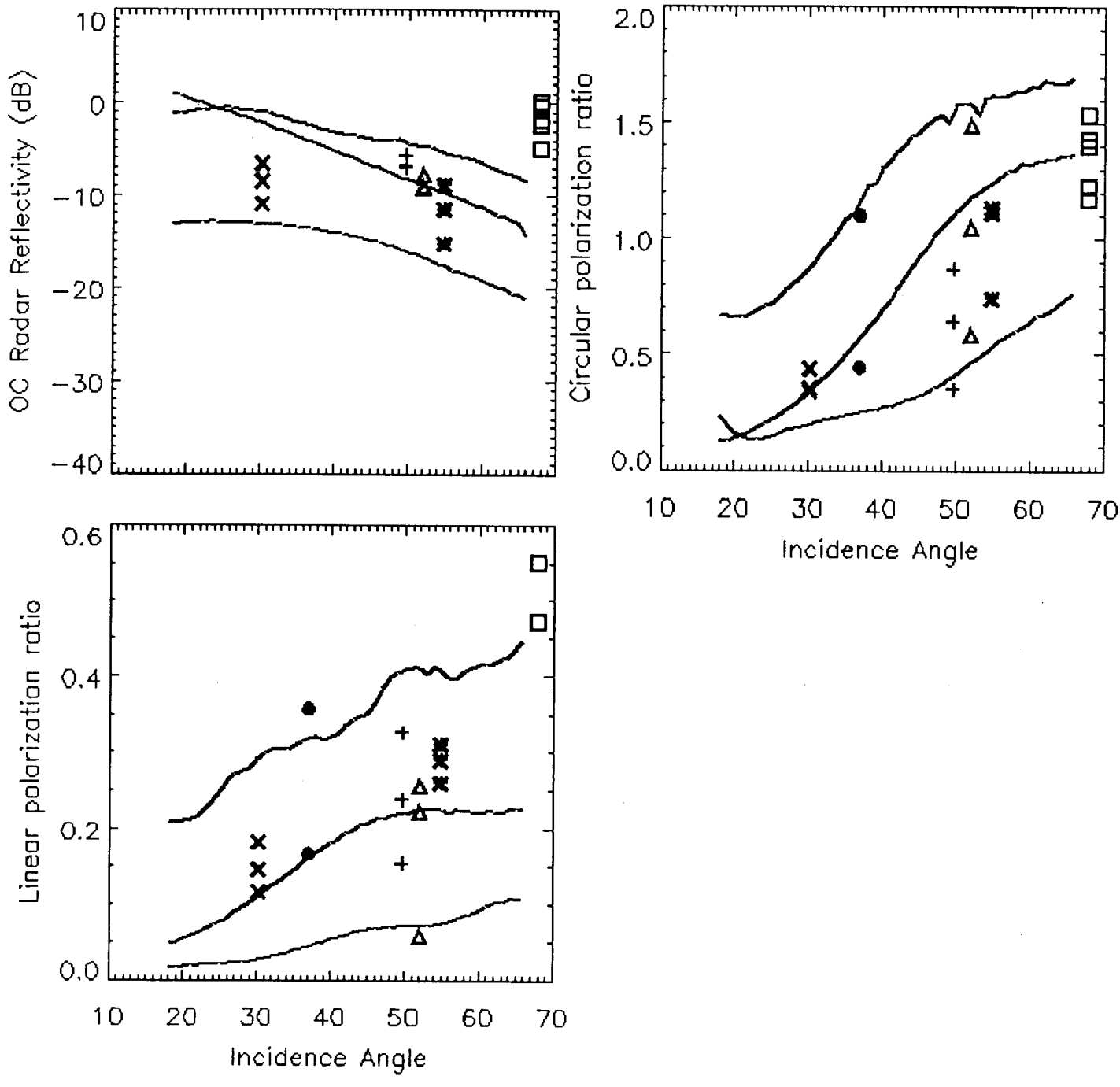

RIGNOT FIGURE 2

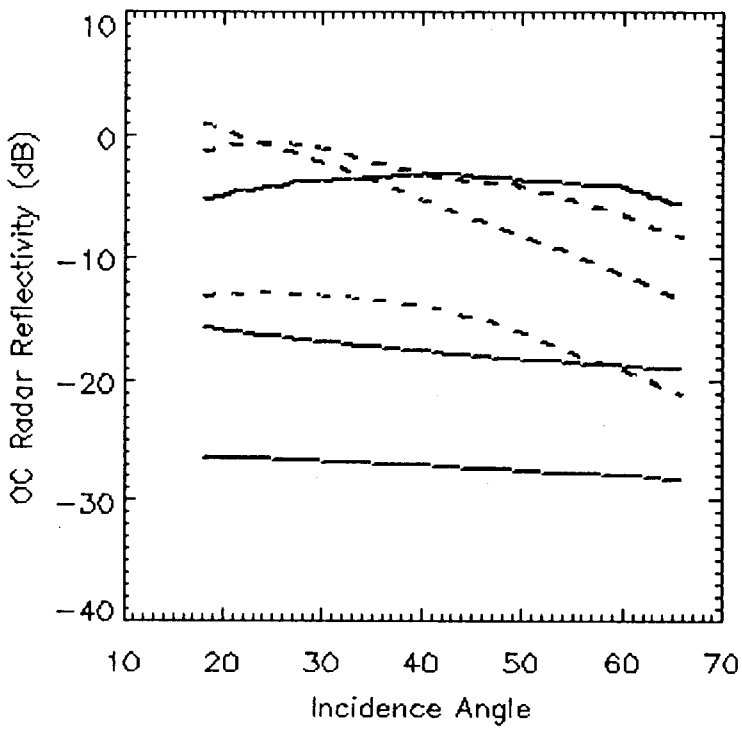

RIGNOT FIGURE 3

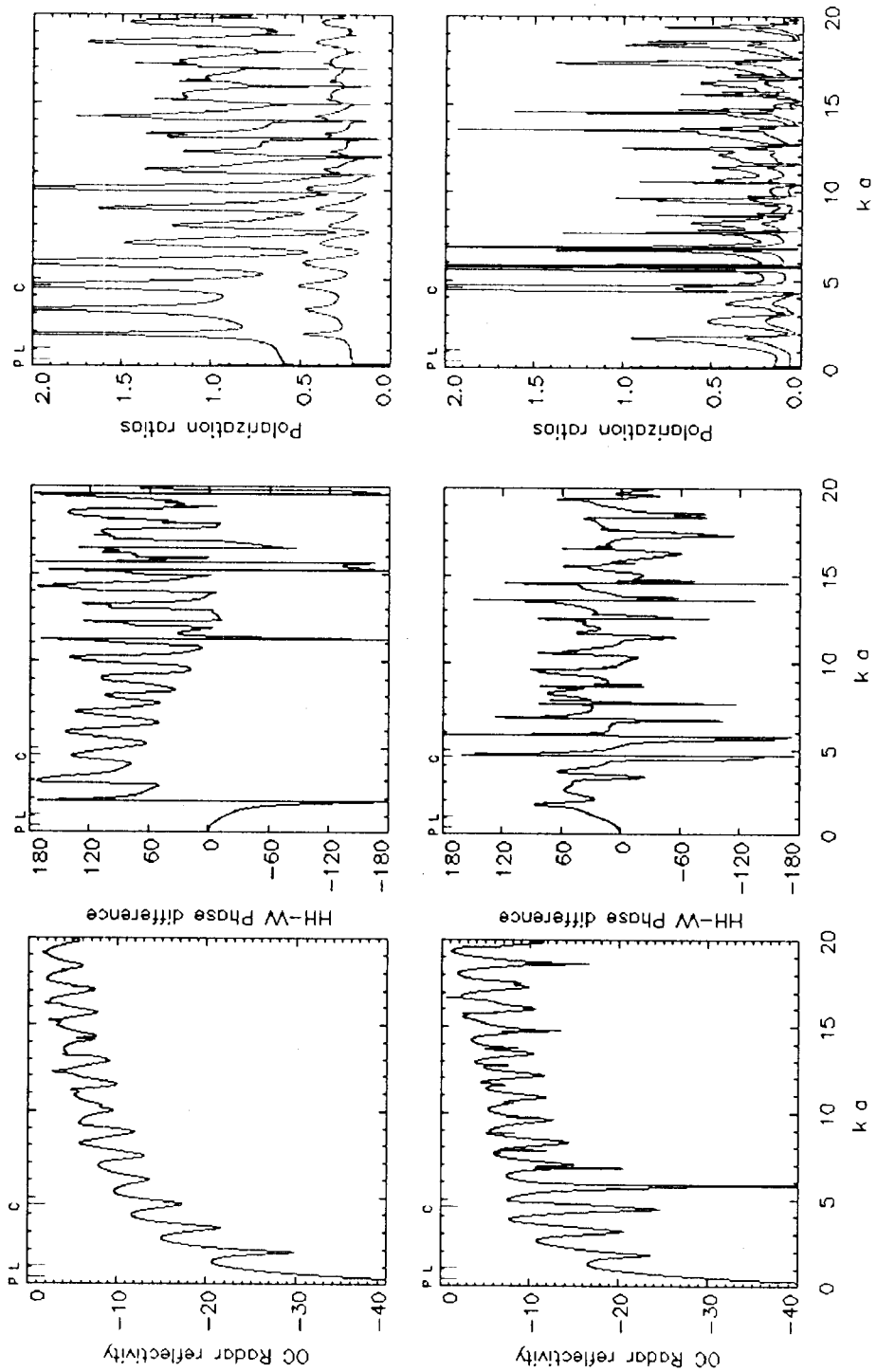

RIGNOT FIGURE 4

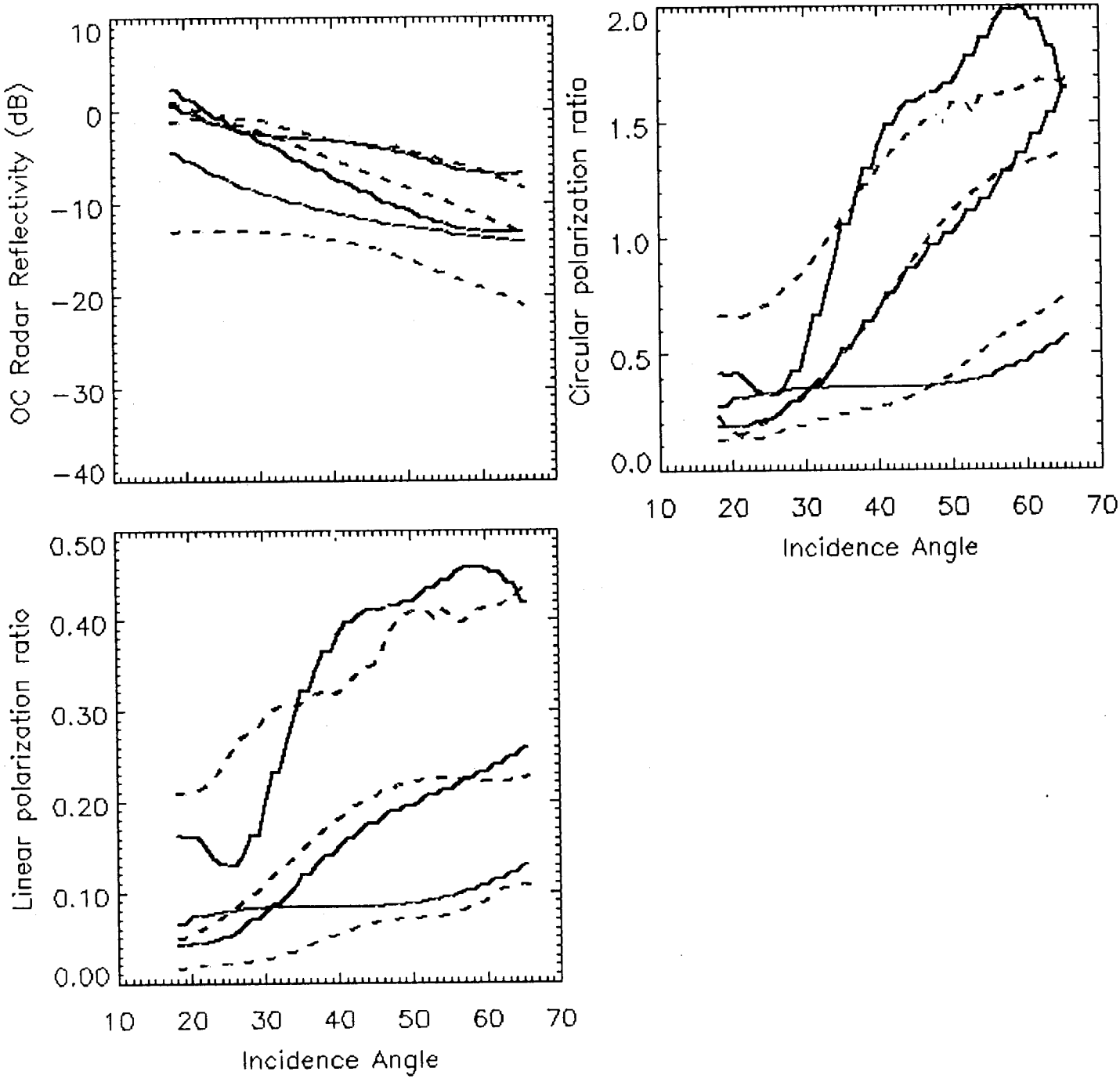

RIGNOT FIGURE 5